MAPPING SOUTH BALTIC NEAR-SHORE BATHYMETRY USING SENTINEL-2 OBSERVATIONS

Gdansk University of Technology, Faculty of Electronics, Telecommunications and Informatics, Department of Geoinformatics, Narutowicza street 11/12, 80-233 Gdansk, Poland. e-mail: andrzej.chybicki@pg.gda.pl

Summary
One of the most promising new applications of remote observations satellite systems (RO) is the near-shore bathymetry estimation based on spaceborn multispectral imageries. In recent years, many experiments aiming to estimate bathymetry in optically shallow water with the use of remote optical observations have been presented. In this paper, the optimal models of satellite derived bathymetry (SDB) for relatively turbid waters of South Baltic Sea were presented. Obtained results were analyzed in terms of depth error estimation, spatial distribution and overall quality. The models were calibrated on the basis of sounding (in-situ) data obtained by single-beam echosounder retrieved from Maritime Office in Gdynia, Poland. The remote observation for this study were delivered by recently deployed European Space Agency Sentinel-2 satellite observation system. A detail analysis of obtained results has shown that both methods can be successfully applied for the region of South Baltic for depths of 12-18 meters, however, significant limitations were observed. Performed experiments, showed that error of model calibration, expressed in meters (RMSE), equals up to 10- 20% of the real depth and generally is case dependent. Therefore, a novel indicator of determining maximal SDB depth was also proposed. What is important, the proposed SDB quality indicator is derived only on the basis of remotely registered data, therefore it can be applied operationally.

1. Introduction

Satellite remote multispectral systems provide valuable large- and local- scale observations of optical and thermal properties of Earth's surface. One of the most promising new applications of remote observation satellite systems (RO) are the near-shore bathymetry estimations. RO observations are an interesting approach because they can provide information on shallow water bathymetry by relatively low-cost in comparison to other known bathymetry retrieval techniques such as Lidar scanning (LS), mutlibeam systems (MBS) and single-beam echosounder (SBE). These methods, particularly LS and MBS, provide high resolution and accurate data, however surveying in this case, is usually expensive and time consuming [1]. With the development of optical and thermal satellite sensors for land and sea observations imagers, new applications of RO arise.

In recent years many experiments aiming to estimate bathymetry in optically shallow waters with the use of remote optical observation have been presented. Basically, two fundamental models of determining bathymetry from optical imagery are defined, namely: empirical optical bands ratio transform algorithm proposed by Stumpf [2] and more analytical approach proposed by Lyzenga [3,4] and Philpot [5]. Both of these models assume that radiation in optical bands is absorbed by water and reflected from the bottom, however this process is observed differently dependently on the wavelength. Therefore, the ratio of observed radiances of at least two optical bands can be used to retrieve the information about the bottom depth.

During this process many factors constitute limitations of these methodologies. When the bottom reflectance and light attenuation of water is stable over the analyzed area, estimates of depth can be relatively easily made by modeling the depth of light penetration based on the amount of reflectance measured by the satellite. Having multiple visible-wavelength spectral bands, the effects of seafloor reflectance variability and water turbidity can be reduced. However, water turbidity is still one of the most important factors in the process of obtaining satellite derived bathymetry (SDB).

Therefore, most of the experiments made in this field are based on testing fields and datasets that satisfy above mentioned criteria. For instance, Sandidge and Holyer used Airborn Visible/Infrared scanner to derive bathymetry for waters of Florida, USA [6]. The observations of optically shallow waters near Bahama islands were also analyzed by Adler-Godlen [7], Sheng Ma [8] and others i.e. [9][10][11][12]. This paper presents the optimal models of satellite based bathymetry derivation developed for the relatively turbid waters of South Baltic Sea. The research involved Sentinel-2 data, log-ratio and analytical

approach that uses inverse transform optimization methods. Results obtained by these two models were then compared in terms of depth error estimation, spatial distribution and quality. The model was calibrated on the basis of sounding (in-situ) data obtained by single-beam echosounder. Calibration data was retrieved from Maritime Office in Gdynia, Poland which is local entity of official Marine Administration in Poland.

2. Methods

Estimation of bathymetry from satellite observations involves extracting the bottom radiance from the measured water-leaving reflectance. Reflectance R is defined as the ratio of the radiance leaving the water surface to the downwelling irradiance just above the water's surface. It is a feature that describes surface optical properties related to the light absorption, scattering properties of the constituents in the water, the bottom albedo and depth. The fundamental physical principle in the process of deriving bathymetry using satellite observations is the phenomena of light pass attenuation in the water column, bottom reflection and scattering (Fig. 1).

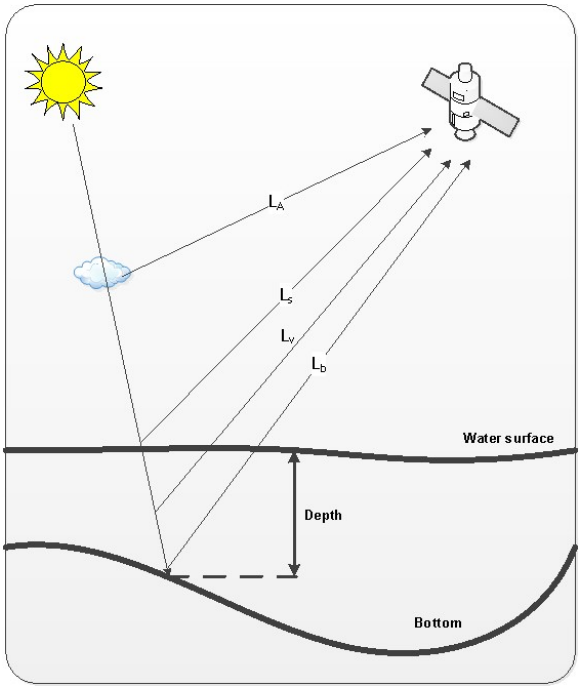

Fig. 1. Physical principle of SDB model

As shown, this can be divided into four basic components of the energy registered at the satellite sensor [13], namely the bottom radiance (L_B), subsurface volumetric radiance (L_v), specular radiance (L_s), and atmospheric path radiance (L_A). This can be written down as follows:

$$L_{TOA} = L_B + L_V + L_s + L_A \qquad (1)$$

radiance registered at the sensor (L_{TOA}) is a sum of atmospheric scattering (L_A), subsurface volumetric radiance (L_v) resulting from volume scattering in the water and its organic/inorganic constituents (e.g. sediment and chlorophyll. Surface radiance (L_S) is caused by reflection of optical energy from the water surface, including possible sunglint effects. The (L_B) is the result of energy reflection from the seabed, which holds the information about bottom scattering characteristics and water depth. In this context, in order to derive bottom depth from satellite observation, disaggregation of bottom and volumetric radiance from total radiance is crucial.

Basically, there are two fundamental models for obtaining SDB. Both of them apply mechanisms of to remove L_p, specular effects, and minimize volumetric scattering effects variability [14][15]. In most approaches this is achieved by assuming that bottom radiance in fully deep water equals zero. Then, total radiance (or reflectance) over optically-deep water (L_∞ or R_∞), represents the combined effects of subsurface volumetric radiance, specular radiance, and atmospheric path radiance. After atmospheric and sunglint corrections, the deep water radiance only contains subsurface volumetric radiance. Assuming that subsurface volumetric radiance in shallow water and atmospheric absorption is the same as that of adjacent deep water, then optically deep water radiance recorded by the remote sensor can be used to correct the subsurface volumetric radiance in shallow water.

In order to minimize errors of depth estimation, possibly largest number of wavelength bands with the smallest attenuation should be used. Maximal derivation depth is limited by water turbidity (caused by suspended sediments, chlorophyll, organic particles) and wavelength registered by the sensor. Therefore the basic band used for SBD is blue light (440 to 540 nm) as it has the smallest attenuation and can penetrate water up to 30m in optimal conditions. Longer wavelengths (green and red) attenuate rapidly in water, green light (500–600 nm) can penetrate to a maximum depth of approximately 15 m, red light (600–700 nm) to 5 m, and near infrared (700–800 nm) to 0.5 m [16].

2.1 Optical bands ratio bathymetry retrieval model

First of the described approaches [3], based on a log-ratio equation, is described by following equation:

$$z_{est} = m_1 \frac{\ln(R(\chi_i))}{\ln(R(\chi_j))} + m_0 \qquad (2)$$

where z_{est} is satellite derived bathymetry depth, m_0 and m_1 are coefficients of the model, $R(\lambda_i)$ and $R(\lambda_j)$ are the remote sensing radiances for optical bands λ_i and λ_j. In this model, the bottom depth is estimated on the basis of light attenuation phenomena, as the attenuation of incoming shortwave radiation varies spectrally, this effect in spectral bands can be observed.

2.2 Analytical inversion model

The local inversion model is derived directly from simplified radiation equation for optically shallow waters (3):

$$L_{TOA} = L_{\infty}[1 - e^{-kz}] + A_d e^{-kz} + L_A + L_s \qquad (3)$$

where A_d is the upwelling spectral radiance directly reflected from the bottom (before interacting with the overlaying water column), k is a two-way attenuation coefficient, and z is depth. In this context, the expression $A_d e^{-kz}$ represents the energy attenuation effect resulting from passing through the water column of known depth z. Assuming that the ratio of bottom reflectance between two spectral bands is constant for all bottom types within a given scene and light attenuation variability caused by atmospheric effects is negligible for a given area, the depth estimated with the use of the following model can be expressed as:

$$z_{est} = \alpha_0 + \sum_{i=1}^{N} \alpha_i \ln[L(\lambda_i) - L_{\infty}(\lambda_i)] \qquad (4)$$

where N is the number of spectral bands, α_i *(i=1,2,...N)* are the constant coefficients derived during model calibration, $L(\lambda_i)$ is the remote sensing radiance after atmospheric and sunglint corrections for spectral band λ_i, The use of natural logarithm in the expression makes the transformation linear to water depth and deepwater-corrected radiances of spectral bands.

3. Materials

In this section, the description of input data for algorithms used in the paper is outlined. Namely, proposed algorithms utilize two types of input datasets: multispectral imageries obtained from Sentinel-2 satellite system that SDB is derived from and calibration dataset constructed from SBE surveys.

3.1 Sentinel-2 data

Sentinel-2 (S2) is a two polar-orbiting satellite system that is the continuation of the SPOT and Landsat series of multispectral missions. It's main objective is to deliver high-resolution optical and thermal operational observations for land/sea monitoring, emergency response and security services [17]. Sentinel-2 is a part European Space Agency (ESA) Copernicus programme and its data is provided via dedicated data dissemination frameworks i.e SciHub [18] or national Copernicus mirror sites [19,20].

Sentinel-2 provides systematic coverage of the globe between 56°S to 84°N, with relatively high revisit frequency (every five days at the equator under the same viewing conditions). The spatial resolution for optical and NIR (865 ± 10nm) bands equals 10m x 10m per pixel. In case of analyzed area, data is delivered in UTM 34N projection grid. Sentinel-2 also delivers six NIR and SWIR bands with 20m x 20m spatial resolution and three 60m resolution bands in optical, NIR and SWIR ranges (Fig. 2).

The observation data from S2 is provided by the mission Ground Segment, that provides processing schemes in four levels:

- Level-0 (L0) - raw compressed geometrically registered data
- Level-1 (L1) - divides into A, B,C and C sub-stages. The letter one, L1C, provides geocoded uncompressed TOA reflectance after radiometric calibration, data correction and geometric refinement.
- Level-2 (L2) stage can be performed with the use of dedicated processing software ([21][22]) and provides bottom of the atmosphere reflectance.

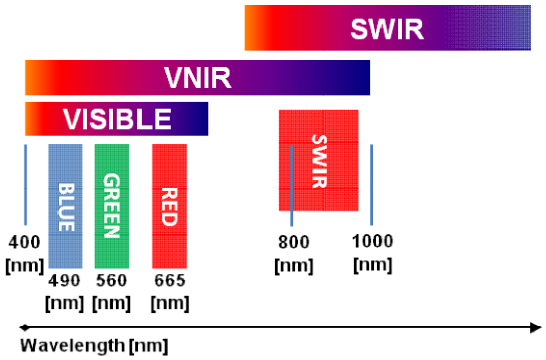

Fig. 2. Sentinel-2 MSI optical bands characteristics.

3.2 Sounding data

Data for SDB model calibration was delivered by Maritime Office in Gdynia (MAG), which is a part of national maritime authority in Poland. Its duties cover such activities as: ensuring and monitoring maritime safety and security in the scope of inspections carried out by Flag State Control and Port State Control, monitoring of ships' traffic and sea routes, and security of ship and port facilities, monitoring of ships' routes and the waterways, management of waters, maritime spatial planning and others.

In addition to above stated duties, MAG performs systematic Polish coast bathymetry surveys using different survey techniques including SBE, MBS and Lidar scanning. Data for presented research was retrieved from near-shore SBE surveys made in 2011. The testing site covers 12 km of south Baltic coast (Fig. 3).

Each survey is based on acoustic sounding profile depth measures, where each sounding within a profile is spaced by 10-20m. Each profile is perpendicular to the coast and starts 1800-2000m before the coastline that corresponds to about 15-20m bottom depth. The profiles are parallel to each other and spaced each 500m along the coast.

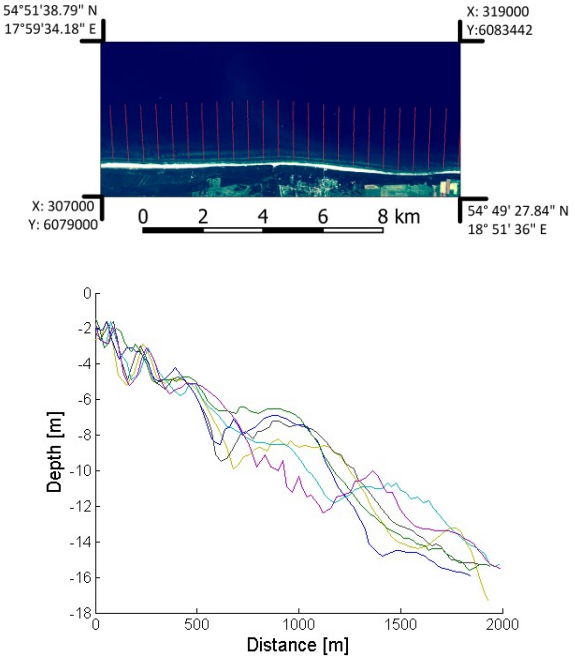

Fig. 3. Calibration test site: upper picture represents the geographically positioned calibration test site on the basis of composite RGB Sentinel-2 imagery in UTM 34N projection. Red dots represent SBE soundings profiles. The lower figure represents plots of selected sounding profiles (the same as on upper figure) in the function of distance from the shore.

4. Results

In order to calibrate the proposed models of bathymetry retrieval, sounding data described in the previous section was used. This process was based on visual and analytical inspection of the calibrating dataset. As it can be observed, sounding in-situ observation contain not only underwater soundings but also some small number of in-situ measurements along the coast (above water surface). Because of this, the in-situ observation with depth less than 0.5 m were removed from further analysis. The remaining data was compared to remote Sentinel-2 observations acquired on *4rd March 2016, 9th March 2016, 27th March 2016,* and *6th May 2016* under clean-sky conditions.

4.1 Log-ratio model calibration

During log-ratio model calibration, for each sounding point a <*observation, model value*>, pair is built. Then, for each pair *model value*, is calculated using eq. (2) with initial $m_0 = 1$ and $m_1 = 0$ values. In the next step, this set of pairs is put under second degree polynomial regression in order to obtain optimal m_0 and m_1 values. The root mean squared error of calibration and correlation is calculated as the quality indicator. The total number of calibration points equals 2074 (Fig. 4). Figures 4-7 show scatter plots of calibrated SDB corresponding to sounding data for different S2 observations performed.

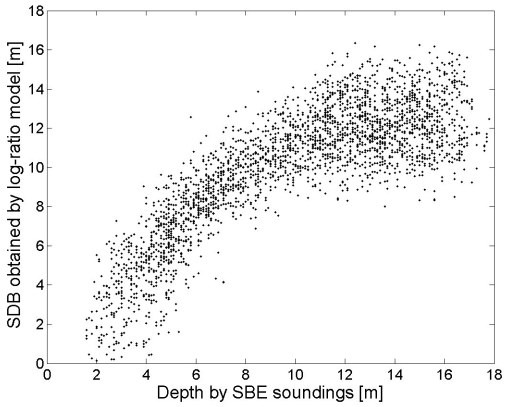

Fig. 4. Scatter plot of results obtained by optimized log-ratio model vs. depths obtained by single-beam (SBE) echosounder. Root mean squared error was RMSE= 2.4231 [m] and Pearson correlation coefficient was R= 0.8254 Model was calibrated on the basis of satellite acquisition made on 4th March 2016.

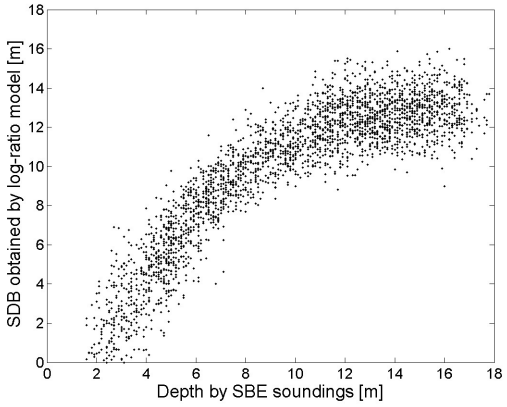

Fig. 5. Scatter plot of results obtained by optimized log-ratio model vs. depths obtained by single-beam (SBE) echosounder. Root mean squared error was RMSE= 2.0555 [m] and Pearson correlation coefficient was R= 0.8779. Model was calibrated on the basis of satellite acquisition made on 9th March 2016.

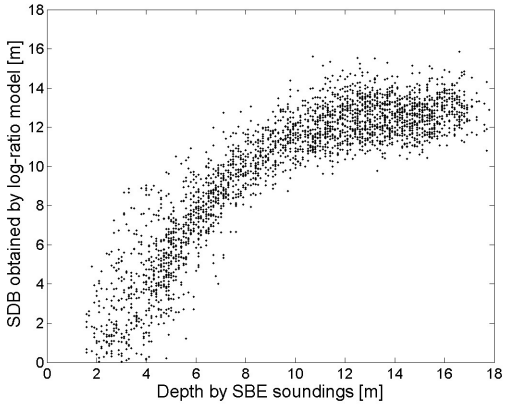

Fig. 6. Scatter plot of results obtained by optimized log-ratio model vs. depths obtained by single-beam (SBE) echosounder. Root mean squared error was RMSE= 2.079 [m] and Pearson correlation coefficient was R= 0.8749. Model was calibrated on the basis of satellite acquisition made on 27th March 2016

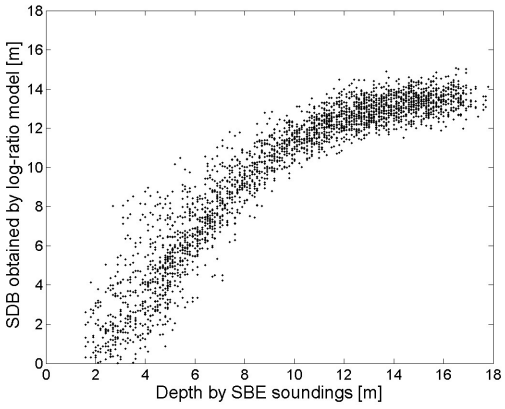

Fig. 7. Scatter plot of results obtained by optimized log-ratio model vs. depths obtained by single-beam (SBE) echosounder. Root mean squared error was RMSE= 1.653 [m] and Pearson correlation coefficient was R= 0.9229. Model was calibrated on the basis of satellite acquisition made on 6th May 2016.

As presented, obtained results indicate strong correlation between obtained SDB and sounding data acquired by SBE. Strong correlation can be particularly observed for mid-range bottom depths. Noise for small bottom depths is caused by optical effects of wave collapse and relatively high temporal bathymetry variation. Depending on the observation, maximal derived bathymetry for deeper sounding differs, however in most cases it ranges between 12 and 16 meters. Within this range of bottom depth values, SBE for deeper optical properties of water become equal to fully deep water.

Nevertheless, it can be seen that for every observation that is used to derive bathymetry, SDB depicts characteristics of the bottom profile lines. In order to present this, selected SBE profiles were plotted together with corresponding SDB profile (Fig. 8). The black line represents calibration data, and coloured lines represent SDB derived along selected SBE profile for different acquisition dates. This result is consistent to previous observations, namely the SDB bathymetry profile depicts the shapes of SBE bathymetry particularly for mid-range bottom depths, and difference between SBE and SDB increases for points deeper than 12-14 meters.

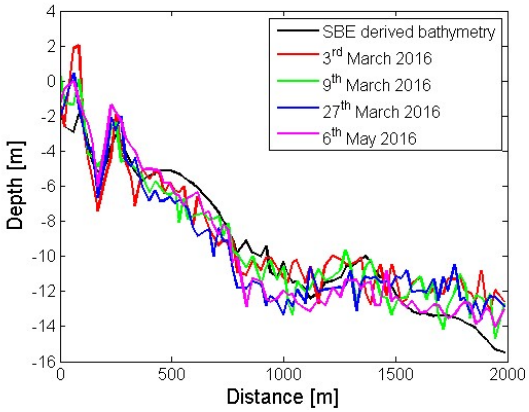

Fig. 8. Comparison of analytical model performance for different calibration dataset for selected SBE profile.

4.2 Analytical model calibration

The methodology for second model calibration was analogical, however this model consist of at least four parameters $(\alpha_0, \alpha_1, \alpha_2, \alpha_4,)$ to be calibrated locally when using Senitnel-2 (3 optical bands - R, G, B were used). Thus, when having M sounding point calibration dataset, eq. 4 is of form:

$$SDB_{M(k)} = \alpha_0 + \sum_{i=1}^{N} \alpha_i \ln[L(\lambda_i)_{M(k)} - L_\infty(\lambda_i)] \qquad (5)$$

where $SDB_{M(k)}$ is a satellite derived bathymetry for k-th sounding point $(M(k))$, where k $(1,2,\ldots,K)$ and K is the total number of calibration points. $L(\lambda_i)_{M(k)}$ is i-th band reflectance corresponding to $M(k)$. Then, for K calibraiton points, optimal solution to above stated optimization problem can be formed as matrix equation (6):

$$\hat{\alpha} = [L^T W L]^{-1} L^T z \qquad (6)$$

where $\hat{\alpha}$ is a N-element column vector of optimal model parameters (α_i), W is optional $K\,x\,K$ weight matrix, L is $K\,x\,N$ matrix, z is K-element column vector of sounding depths. Figures 9-12 represent analogical scatter plots of calibrated SDB depths against SBE data. Generally, the results are consistent with previous case, however some significant conclusions can be derived. For instance, both models reach similar maximum depth derivation that ranges in about 12-16 meters. It can be also observed that higher noise in data occurs for small- and maximum-depth ranges, while in mid-depth ranges noise is relatively smaller. Moreover, in both cases, SDB obtained from observation made on 6th May 2016, results in smallest error among all observations. That leads to the conclusion, that low water turbidity and other obscuring effects have higher impact on final quality of SDB then the applied model.

.

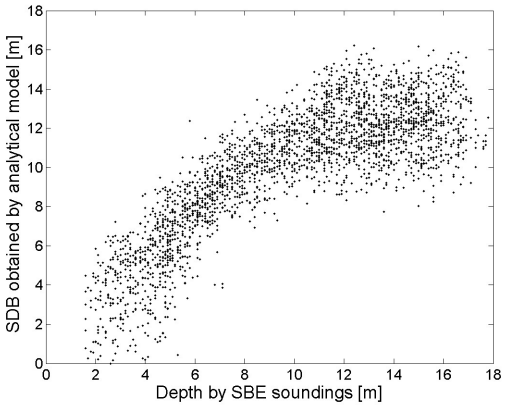

Fig. 9. Scatter plot of results obtained by optimized analytical model vs. depths obtained by SBE. Root mean squared error was RMSE= 2.4186 [m] and Pearson correlation coefficient was R= 0.8262. Satellite acquisition made on 4th March 2016.

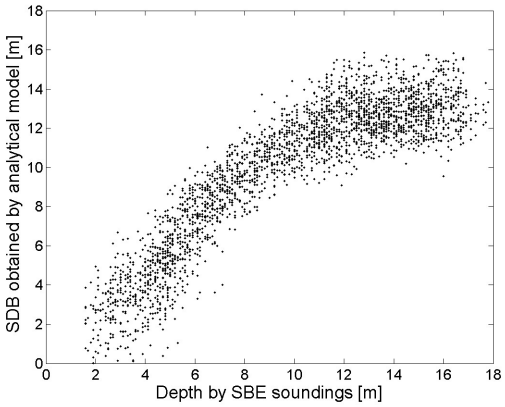

Fig. 10. Scatter plot of results obtained by optimized analytical model vs. depths obtained by SBE. Root mean squared error was RMSE= 1.9694 [m] and Pearson correlation coefficient was R= 0.885. Model was calibrated on the basis of satellite acquisition made on 9th March 2016.

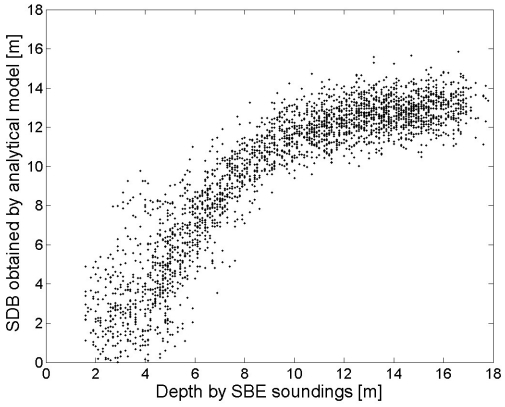

Fig. 11. Scatter plot of results obtained by optimized analytical model vs. depths obtained by single-beam (SBE) echosounder. Root mean squared error was RMSE= 1.9727 [m] and Pearson correlation coefficient was R= 0.8881. 9th March 201. Model was calibrated based on satellite acquisition made on 27th March 2016.

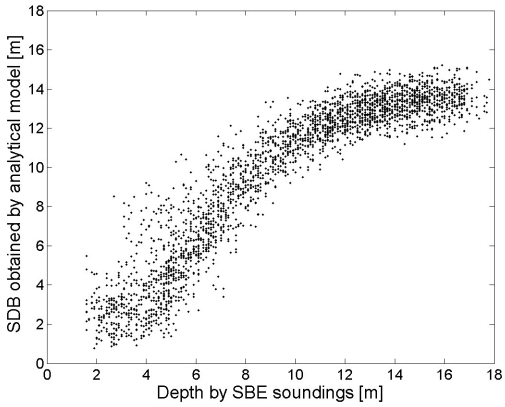

Fig. 12. Scatter plot of results obtained by optimized analytical model vs. depths obtained by single-beam (SBE) echosounder. Root mean squared error was RMSE= 1.651 [m] and Pearson correlation coefficient was R= 0.9231. Model was calibrated on the basis of satellite acquisition made on 6th May 2016.

Detailed comparison of SDB and SBE on the example of selected SBE profile (the same as in previous case) is presented in Fig. 13. In this case, similar conclusions related to SDB errors and maximum derivation depth can be derived, however additional issues should be discussed. Firstly, both models can be characterized by the repeatability of obtained SDB profiles. Shapes of SBE bottom profiles can be observed in both log-ratio and analytical, models' results, and this is observable for all acquisitions. However, on both models, very shallow SDB observation can be derived to be over water surface - this can be particularly observed for observation made on 3rd March 2016. However, there is no certain method to tell whether this information is true or false. In other words, for this particular observation, some areas very near to the shore could be exposed above water surface due to low tide or past storm.

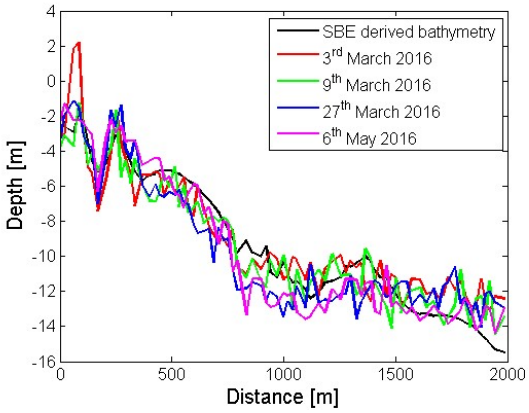

Fig. 13. Comparison of analytical model performance for different calibration datasets for one selected SBE profile.

Overall comparison of model performance for different S2 observations is given in Table 1. This analysis shows, that both models obtain satisfactory quality of SDB for depths 0-16m. This comparison also confirms conclusions made earlier that the observation presented

in the 4th row of the table (6th May 2016) is characterized by the highest quality what is confirmed by the lowest RMSE (1.653 m for log-ratio model and 1.653 m for analytical model) and highest correlation from all calibration datasets (0.9229 and 0.9231 respectively).

Tab. 1. Comparison of model performance after calibration with different acquisition datasets

	Log-ratio model		*Analytical model*	
Acquisition date	***R***	***RMSE***	***R***	***RMSE***
04.03.2016	*0.8254*	*2.4231*	*0.8262*	*2.4186*
09.03.2016	*0.8779*	*2.0555*	*0.885*	*1.9694*
27.03.2016	*0.8749*	*2.079*	*0.8881*	*1.9727*
06.05.2016	*0.9229*	*1.653*	*0.9231*	*1.651*

4.3 Error analysis

As it was observed, correlation between SDB and SBE bathymetry is clearly visible, particularly for the depths less than approximately 16 meters. For deeper soundings, SDB estimator becomes constant and uncorrelated as for fully deep water. In this context, it is worth to notice that SDB models don't behave evenly for all bottom depths and model calibration is not efficient for the depths higher than 12-16 meters. Therefore, model calibration using calibration points deeper than a particular threshold worsens general model performance.

In order to analyze how bottom depth influences the error of SDB, additional analysis of obtained results was performed. For each remote observation bathymetry error analysis was plotted as the function of depth. Results of these analysis are given in Fig. 14-17. In each figure, the upper plot represents the error of SDB in the function of depth, the middle graph represents the number of calibration points for each of water depth bins (it is a depth histogram of calibration dataset). The lower area contains the plot of newly introduced SDB quality coefficient (SDB_{Qcoef}) that describes quality of retrieved SBD described by the following formula:

$$SDB_{Qcoef} = \frac{\ln(1 + R(\lambda_i))}{\ln(1 + R(\lambda_j))} - (\ln[\frac{1 + R_\infty(\lambda_i)}{1 + R_\infty(\lambda_j)}] - 2\sigma) \qquad (7)$$

where σ is standard deviation of selected field with fully deep water log ratios reflectance for λ_i and λ_j wavelengths. SDB_{Qcoef} enables to determine a threshold value to which bathymetry derived by proposed models can be retrieved with the certain quality. Note that this value is only dependent on remote observation data, therefore no bathymetric or other auxiliary information is necessary to compute it. Therefore, it can be used operationally. The red line in the lower plots (Fig. 14-17) represents 0 value threshold. As it can be observed when SDB_{Qcoef} reaches the threshold, SDB error is clearly increasing

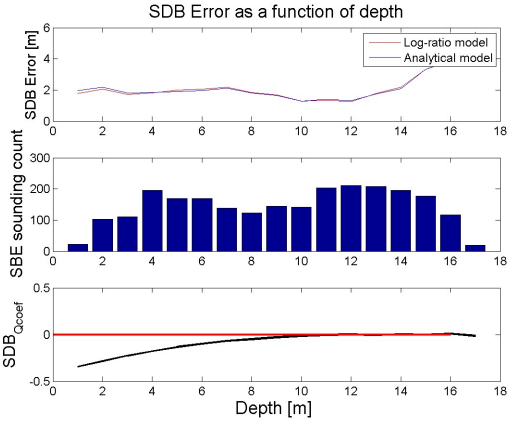

Fig. 14. Error distribution in function of depth (upper picture), SBE sounding count (middle), and SDB quality indicator plot (lower) for 4th March 2016. The red line in the lower plot represents 0 value threshold.

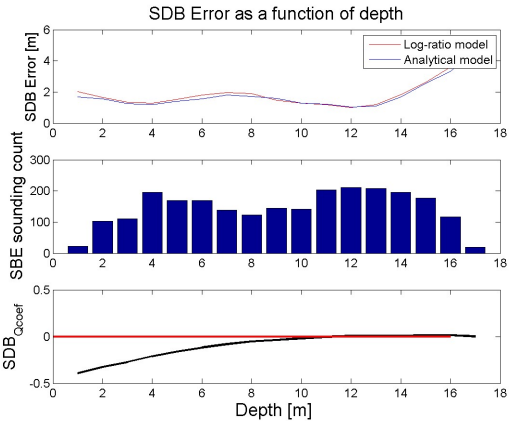

Fig. 15. Error distribution in function of depth (upper picture), SBE sounding count (middle), and SDB quality indicator (SDB_{Qcoef}) plot (lower) for 9th March 2016

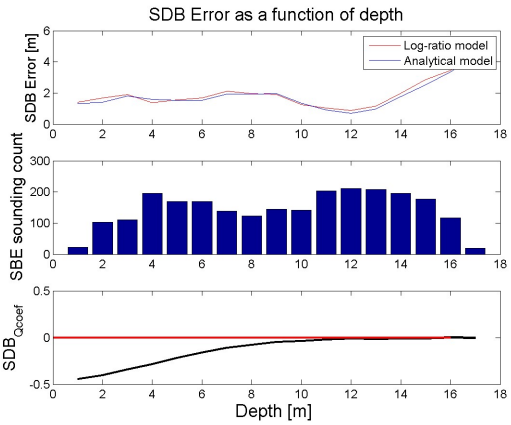

Fig. 16. Error distribution in function of depth (upper picture), SBE sounding count (middle), and SDB quality indicator (SDB_{Qcoef}) plot (lower) for 27th March 2016

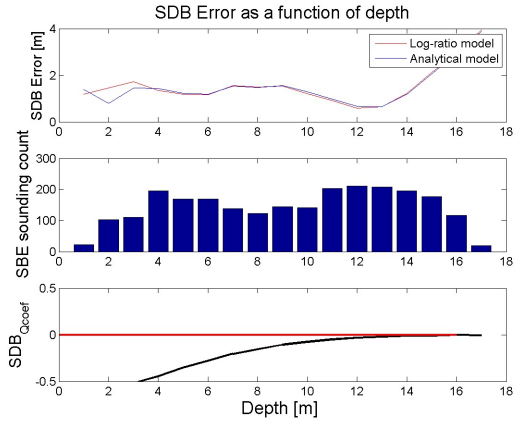

Fig. 17. Error distribution in function of depth (upper picture), SBE sounding count (middle), and SDB quality coefficient (SDB_{Qcoef}) indicator plot (lower) for 6th May 2016

In order to show benefits of using SDB_{Qcoef} threshold, each model was calibrated with only those observations which met the aforementioned quality criterion, namely where $SDB_{Qcoef} < 0$. In this way, during model calibration only those observations that were indicated as valid by the quality indicator, were used. The results of model calibration, presented in Tab. 2, show significant improvement of quality indicators. Namely, for every observation dataset RMSE values are significantly lower: for log-ratio model RMSE was reduced from 1.653-2.4231[m]range to 1.0822 -1.4319 [m] range and in case of analytical model reductions equals 1.0681-1456[m] from 1.651-2.4186 [m]. Analogically, correlation coefficient increase could be observed from 0.8254-0.9229 to 0.8736-0.9346 in case of log-ratio model and from 0.8262-0.9231 to 0.869-0.9345 in case of analytical model.

Tab. 2. Comparison of model performance after calibration with different acquisition datasets of SDB with maximal depth determined by the quality indicator (SDB_{Qcoef}).

	Log-ratio model		*Analytical model*	
Acquisition date	***R***	***RMSE***	***R***	***RMSE***
04.03.2016	***0.8736***	***1.4319***	***0.869***	***1.456***
09.03.2016	***0.9065***	***1.0822***	***0.9091***	***1.0681***
27.03.2016	***0.9083***	***1.3678***	***0.9115***	***1.3447***
06.05.2016	***0.9346***	***1.3632***	***0.9345***	***1.3643***

4.4 Results verification

In order to perform visual inspection of bottom maps generated by the proposed SDB models and visually verify the quality of proposed SBD models, maps representing bathymetry derived from remote observations were generated. Figures 18-21 represent the SDB obtained with the use of log-ratio and analytical model. Data is presented in color coded depth ranging from 0 to 18 meters. Model was calibrated with the use of SDB_{Qcoef} thresholding technique, described in previous sections. Areas above water surface, in SDB and coast, were marked as white pixels.

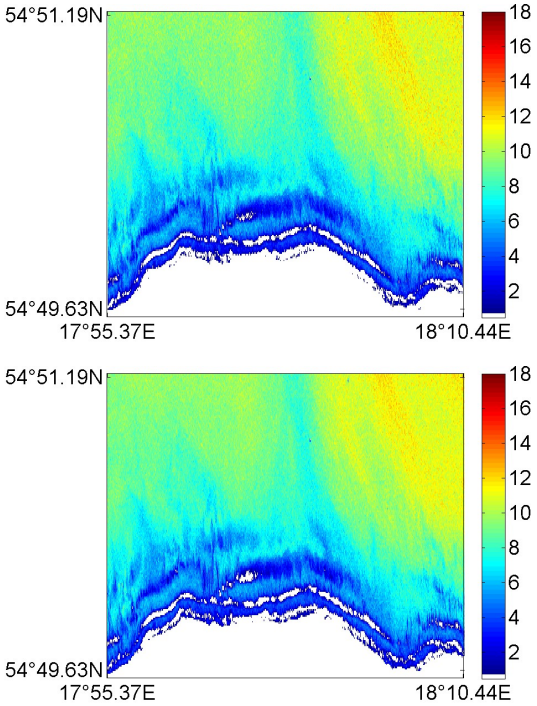

Fig. 18. Comparison of colour coded depth maps obtained by optimized log-ratio SDB model (upper figure) and analytical SDB model (lower figure) for the 3rd March 2016.

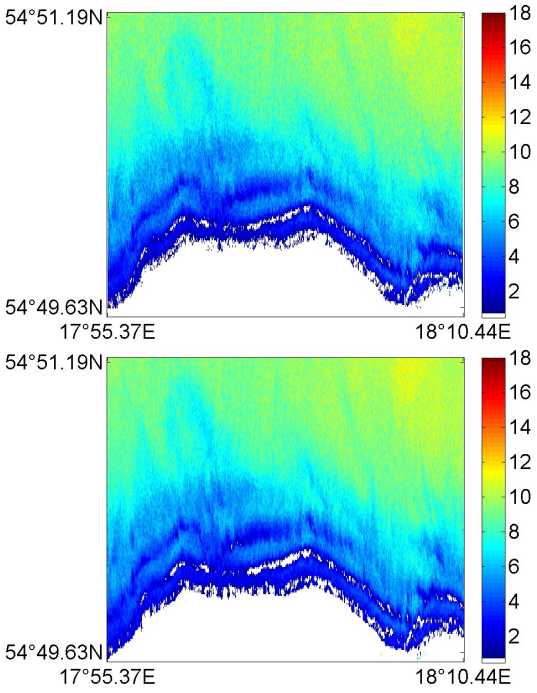

Fig. 19. Comparison of colour coded depth maps obtained by optimized log-ratio SDB model (upper figure) and analytical SDB model (lower figure) for the 9th March 2016.

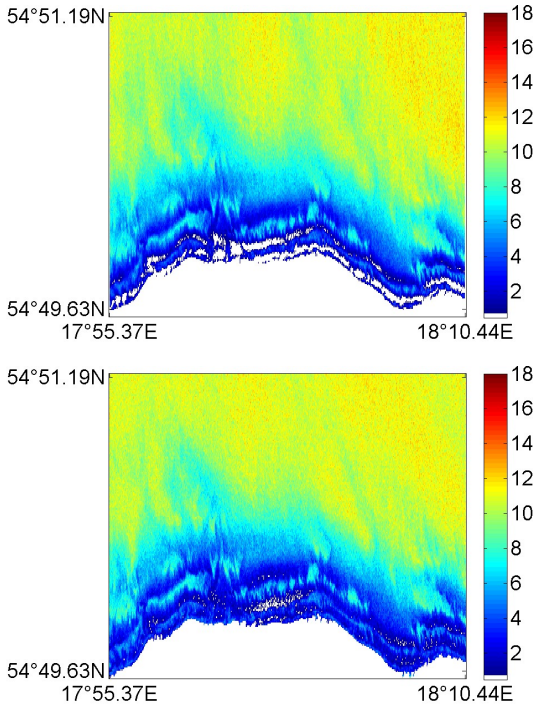

Fig. 20. Comparison of colour coded depth maps obtained by optimized log-ratio SDB model (upper figure) and analytical SDB model (lower figure) for the 27th March 2016. White pixels represent depth derived as above the sea surface.

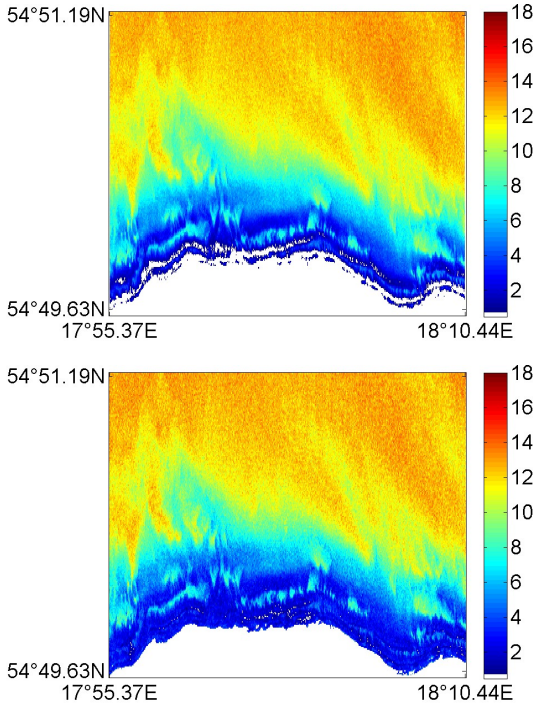

Fig. 21. Comparison of colour coded depth maps obtained by optimized log-ratio SDB model (upper figure) and analytical SDB model (lower figure) for the 6h May 2016. White pixels represent depth derived as above the sea surface.

It can be observed that depth maps retrieved from both models are relatively similar, and both techniques obtain similar results in the context of visual analysis. Visible noises observed in scatter plots presented in previous sections (Fig. 4-11) are also noticeable in maps. Visual inspection of the results, also reveals the fact that methods behave relatively poorly for depths exceeding maximum derivation depth determined by the SDB_{Qcoef} factor. However, for shallow and non-turbid waters even single 3D shapes of underwater bathymetry are easy to retrieve for human eye.

On the basis of visual inspection, only minor differences between the observations acquired at the same time are noticeable and both methods can be used for these relatively turbid and difficult conditions.

5. Conclusions

In the paper, two fundamental methods for bathymetry retrieval from S2 multispectral satellite observations were compared. Results were obtained on the basis of data acquired for 12-km long south Baltic coastline and the calibration points were acquired from SBE surveys and were delivered by National Maritime Administration.

A detail analysis of obtained results shows that both methods can be successfully applied for the region of South Baltic, however, some limitations and factors causing obstruction of the results can be observed. The most important in this case is the water turbidity, therefore, the bathymetry can be derived approximately to depths of 12-18 meters. What is more important is the fact that maximum depth, that can be derived from satellite observation, varies in time and space and is difficult to be assumed a priori. Therefore, a novel indicator of determining maximal SDB depth was proposed in the paper. The proposed SDB quality indicator is derived only on the basis of remotely registered data, therefore it can be applied operationally.

During the research, detail analysis of errors obtained for different depths ranges was also performed. Obtained results indicate that the error of model calibration, expressed in meters (RMSE), equals up to 10- 20% of the real depth and generally is case dependent. This value is worse than results obtained by other authors [1-15], however, there are at least two reasons for this: firstly, the water turbidity, effects of light attenuation and it's spatial variety is much more obscuring in case of Baltic Sea than in other locations such as presented in [1-15], where testing datasets were related to optically clear waters. Another issue is that bathymetry surveys for this research were not collected at the same time. This is because of the fact, that Polish Maritime office performs SBE surveys periodically and so exact time co-incidence between remote observation and calibration data acquisitions was unfortunately no available for our test site. Nevertheless, it was shown that proposed methods, combined with SDB quality indicator, are not only self adaptive but can be also used operationally for instance for delivering cost effective alternative for large scale bathymetry

observations. The novelty of work presented in the paper also relies on the fact that research is based on newly deployed ESA Sentinel-2 observations obtained for relatively difficult turbid Baltic waters.

Acknowledgements

The author wish to thank Maritime Office in Gdynia, Poland for providing sounding bathymetry maps used in the research presented in the paper.

References

[1] . D. R. Lyzenga, N. R. Malinas, and F. J. Tanis, "Multispectral bathymetry using a simple physically based algorithm," IEEE Trans. Geosci. Remote Sens., vol. 44, no. 8, pp. 2251–2259, Aug. 2006.

[2] Stumpf, R.P., Holderied, K., Sinclair, M., 2003. Determination of water depth with high-resolution satellite imagery over variable bottom types. Limonology Oceanogr. 48, 547–556. doi:10.4319/lo.2003.48.1_part_2.0547

[3] R.Lyzenga, D., 1981. Remote sensing of bottom reflectance and water attenuation parameters in shallow water using aircraft and Landsat data. Int. J. Remote Sens. 2, 71–82.

[4] R. Lyzenga, D., 1978. Passive remote sensing technique for mapping water depth. Appl. Opt. 17, 379–383.

[5] Philpot, W.D., 1989. Bathymetric mapping with passive multispectral imagery. Appl. Opt. 28, 1569–1578. doi:10.1364/AO.28.001569

[6] J. C. Sandidge, and R. J. Holyer, "Coastal bathymetry from hyperspectral observations of water radiance," Remote Sens. Environ., vol. 65, no. 3, pp. 341–352, Sep. 1998.

[7] . S. M. Adler-Golden, P. K. Acharya, A. Berk, M. W. Matthew, and D. Gorodetzky, "Remote bathymetry of the littoral zone from AVIRIS, LASH, and QuickBird imagery," IEEE Trans. Geoscis. Remote Sens., vol. 43, no. 2, pp. 337–347, Feb. 2005.

[8] Sheng Ma, Zui Tao, Xiaofeng Yang, Member, IEEE, Yang Yu, Xuan Zhou, and Ziwei Li, " Bathymetry Retrieval from Hyperspectral Remote Sensing Data in Optical-Shallow Water", Ieee Transactions On Geoscience And Remote Sensing, Vol. 52, No. 2, February 2014

[9] H. Holden and E. LeDrew, "Measuring and modeling water column effects on hyperspectral reflectance in a coral reef environment," Remote Sens. Environ., vol. 81, nos. 2–3, pp. 300–308, Aug. 2002.

[10] Haibin Su, , Hongxing Liu, William D. Heyman, "Automated Derivation of Bathymetric Information from Multi-Spectral Satellite Imagery Using a Non-Linear Inversion Model", Marine Geodesy, vol. 31, 2008.

[11] E. P. Green, P. J. Mumby, A. J. Edwards, and C. D. Clark, "Remote sensing handbook for tropical coastal management," in Coastal Management Sourcebooks 3, A. J. Edward, Ed. Paris, France: UNESCO, 2000.

[12] Poliyapram V., Venkatesh R., Shinji M., 2016, Satellite-derived bathymetry using adaptive geographically weighted Regression model, Marine Geodesy, vol. 39:6, 458-478.

[13] Jensen, J. R. 2007. Remote sensing of the environment: An earth resource perspective, 2nd ed. Upper Saddle River, NJ: Prentice Hall

[14] Mishra, D., S. Narumalani, D. Rundqulst, and M. Lawson. 2006. Benthic habitat mapping in tropical marine environments using QuickBird multispectral data. Photogrammetric Engineering & Remote Sensing 72:1037–1048.

[15] Lyzenga, D. R., N. P. Malinas, and F. J. Tanis. 2006. Multispectral bathymetry using a simple physically based algorithm. Geoscience and Remote Sensing, IEEE Transactions on 44:2251–2259.

[16] Green, E. P., P. J. Mumby, A. J. Edwards, and C. D. Clark. 2000. Remote sensing handbook for tropical coastal management. Paris: A. J. Edwards, UNESCO

[17] Drusch, M. & 14 co-authors (2012). Sentinel-2: ESA's optical high-resolution mission for GMES operational services, Rem. Sens. Env. (accepted).

[18] Sentinels Scientific Data Hub, Technical Guide, European Space Agency, source: https://scihub.copernicus.eu/userguide/ (accessed on 22/12/2016)

[19] Hellenic National Sentinel Data Mirror Site. Operated by the National Observatory of Athens. Source: https://sentinels.space.noa.gr/ (accessed on 22/12/2016)

[20] National French Copernicus Site, Centre National D'Etudes Spatiales, Source: https://copernicus.cnes.fr/en/ground-segment-1 (accessed on 22/12/2016)

[21] Sentinel Application Platform (SNAP), available at Science Toolbox Exploitation Platform (STEP), European Space Agency, source: http://step.esa.int/main/toolboxes/snap/ (accessed on 22/12/2016)

[22] Sen2cor - Sentinel-2 Level 2A product generation and formatting, available at Science Toolbox Exploitation Platform (STEP), European Space Agency, source: http://step.esa.int/main/third-party-plugins-2/sen2cor/ (accessed on 22/12/2016)